Mechatronic Design and Control of a Rigid-Soft Hybrid Knee Exoskeleton for Gait Intervention

Zilu Wang, Zhihao Zhou, *Member, IEEE*, Lecheng Ruan, Xiaojie Duan, and Qining Wang, *Senior Member, IEEE*

***Abstract*—Knee exoskeletons have gained increasing attention for gait training and intervention. The effectiveness of conventional rigid exoskeletons is degraded by bulkiness, high inertia, and joint misalignment. The soft configurations relax the constraints on the knee joint, thus circumvent the misalignment issue, and reduce the system size and weight. However, the soft exoskeletons sacrifice the load sharing capability from rigid support, and also the mechanical stop for constraining joint working range to avoid unsafe knee hyperextension. This article presents a novel rigid-soft hybrid exoskeleton to provide bidirectional interventions safely for knee joint motion. The design is lightweight (1.2 kg to wear), avoids the rigid rotation center that induces knee joint misalignment, has minimal impact on normal walking kinematics, and is able to provide support to the human body. A gait intervention strategy is designed under the hybrid model of human and exoskeleton. Comprehensive experiments are conducted to demonstrate the capability of the presented exoskeleton on gait intervention.**

***Index Terms*—Cable-driven linear actuator, gait intervention, rigid-soft hybrid structure, knee exoskeleton.**

Manuscript received 30 October 2022; revised 16 January 2023; accepted 8 February 2023. Date of publication 1 March 2023; date of current version 17 October 2023. Recommended by Technical Editor H. Wang and Senior Editor G. Alici. This work was supported in part by the National Natural Science Foundation of China under Grant 52005011 and Grant 51922015, in part by the Beijing Municipal Science and Technology project under Grant D181100000318002, and in part by PKU-Baidu Fund under Grant 2020BD008. *(Zilu Wang and Zhihao Zhou contributed equally to this work.) (Corresponding author: Qining Wang.)*

This work involved human subjects or animals in its research. Approval of all ethical and experimental procedures and protocols was granted by the local ethics committee of the First Hospital, Peking University, China (under Application No. D181100000318002).

Zilu Wang is with the College of Engineering, Peking University, Beijing 100871, China (e-mail: ziluwang@pku.edu.cn).

Zhihao Zhou is with the Institute for Artificial Intelligence, Peking University, Beijing 100871, China, and also with the Beijing Engineering Research Center of Intelligent Rehabilitation Engineering, Beijing 100871, China (e-mail: zhouzhihao@pku.edu.cn).

Lecheng Ruan is with the Beijing Institute for General Artificial Intelligence (BIGAI), Beijing 100080, China, and also with the National Key Laboratory of General Artificial Intelligence, Beijing 100080, China (e-mail: ruanlecheng@bigai.ai).

Xiaojie Duan is with the College of Future Technology, Peking University, Beijing 100871, China, and also with the Beijing Engineering Research Center of Intelligent Rehabilitation Engineering, Beijing 100871, China (e-mail: xjduan@pku.edu.cn).

Qining Wang is with the Department of Advanced Manufacturing and Robotics, College of Engineering, Institute for Artificial Intelligence, Peking University, Beijing 100871, China, also with the University of Health and Rehabilitation Sciences, Qingdao 266071, China, and also with the National Key Laboratory of General Artificial Intelligence, BIGAI, Beijing 100080, China (e-mail: qiningwang@pku.edu.cn).

This article has supplementary material provided by the authors and color versions of one or more figures available at https://doi.org/10.1109/TMECH.2023.3245810.

Digital Object Identifier 10.1109/TMECH.2023.3245810

I. Introduction

KNEE exoskeletons have been widely investigated for medical applications, especially in the area of gait training and intervention, to actively assist normal walking and regulate gait [1], [2], [3]. This requires the exoskeleton to be able to intervene in the motion of human knee joints and lower limbs during human gait. Accordingly, two major configurations of such exoskeletons have been proposed. The rigid configuration establishes a rigid structure and robotic joint to mimic the human skeleton system, and a rigid transmission system for the functionalities of human muscles [4]. Apart from driving bidirectional joint motions, the rigid structure is also capable of sharing joint load, which can meet the requirements of some kinds of patients. However, the system rigidity also introduces bulkiness and large inertia, which degrades the easiness of normal walking for wearers [5].

Another major concern for the rigid configuration is that the design of the exoskeleton joint is oversimplified. The human knee joint operates approximately under a crossed four-bar linkage model that contains posterior cruciate ligament, anterior cruciate ligament, tibia, and femur [6]. The joint rotation center and axis vary along the nonuniform joint surface in six degrees-of-freedom (DoFs) at different angles [7]. When designing the knee exoskeleton, however, the joint structure is simplified by either a hinge with one flexion-extension DoF [8], [9], [10], [11], [12], [13], or a double-gear meshing system [14], of which both cause misalignment to the human knee motions and thus affect the normal walking of wearers and hinder the rehabilitation [15]. Several studies attempted to address this issue by designing self-alignment joint mechanisms or adding passive DoFs [16], [17], [18], [19], [20], or using curved guide rail [21], but those designs only work on sagittal plane and/or frontal plane and meanwhile add extra weight. In addition, the migration of the exoskeleton along the leg due to its large weight also leads to misalignment [22].

The bulkiness, large inertia, and joint misalignment of rigid knee exoskeletons collectively motivate the development of soft knee exoskeletons [23], [24], [25], [26]. The most noteworthy feature is robotic joint-free design, typified by exosuit [5]. The

driving forces are exerted on the human joint by active cables anchored to soft fabrics tightened on the limbs, which better facilitates the human knee joint movements while effectively reducing the size and inertia; thus, it less hinders normal walking during usage [5]. However, this design generally provides joint torque in one direction and sacrifices the load sharing capability of the rigid exoskeletons. Meanwhile, safety concern arises from the joint-free design. While rigid exoskeletons can easily constrain the joint range for active operation by integrating a mechanical stop into the exoskeleton joint, the joint-free nature of the soft exoskeletons makes implementation of such protection challenging [23]. Operations outside the proper joint range can induce knee hyperextension and thus severe injury to the subject. In existing works, this safety concern for the soft exoskeletons is usually merely addressed in the control software [23]. Mechanical protection, as such in the rigid configurations, has not been successfully applied on the joint-free exoskeletons.

To address these challenges, the desired knee exoskeleton for gait training and intervention should gather the advantages of soft configurations, e.g., compactness, lightweight, small inertia, and minimal impact on normal gait kinematics, while safety and being able to provide bidirectional joint torque and support ability as the rigid configurations. This article proposes a rigid-soft hybrid configuration, which can provide gait intervention to the wearers while avoiding bulkiness, knee hyperextension, and knee joint misalignment to retain the easiness and safety of normal walking. Preliminary results have been partially presented in [27]. The main works of this article lay in the systematic process for components and parameter optimization, safety design, a complete control strategy for gait intervention under the human-exoskeleton hybrid kinematic model, and comprehensive experiments to verify its effectiveness on gait intervention, and minimal impact on normal gait kinematics during operation.

II. Rigid-Soft Hybrid Exoskeleton

The desired knee exoskeleton for gait training and intervention, as concluded in the previous section, should be able to provide bidirectional torque to the knee joint, while being light-weighted and compact, capable of sharing joint load and supporting human body, and having minimal impact on normal walking. This section proposes a rigid-soft hybrid configuration for exoskeleton design, to address the aforementioned issues by composing the cuffs with a cable-driven linear actuator, as shown in Fig. 1. The linear actuator provides bidirectional force (and support) to the human limb and knee joint through the cuff and is driven remotely by cables to reduce the weight and size of the wearable component. The circumvention of rigid exoskeleton structure with robotic joint releases the six DoFs variation of knee joint rotation center and axes. By virtue of the system's conceptual design, the total weight of the wearable component is constrained within 1.2 kg, which is lightweight for the wearable robotic system. The design methodology in this proposed platform can be easily extended to other lower-limb exoskeletons.

The proposed rigid-soft hybrid knee exoskeleton system (Hybrid-KEX) can be functionally divided into two subsystems:

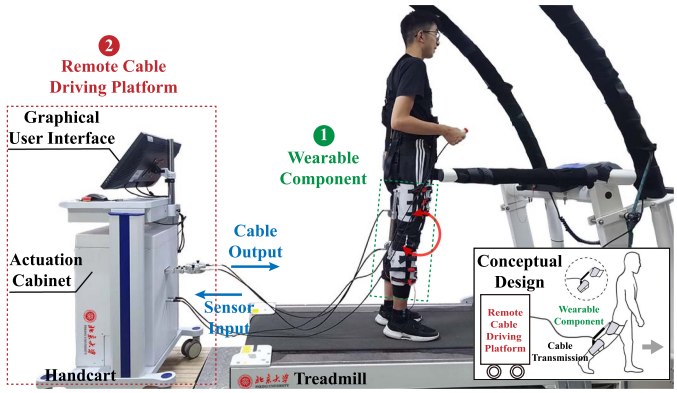

Fig. 1. Proposed rigid-soft hybrid knee exoskeleton prototype. It can be divided into two subsystems: 1) wearable component with linear actuator donned on the human body and 2) remote cable driving platform behind the human body which was integrated with graphical user interface, cable driving unit, control hardware, sensor acquisition, and battery management.

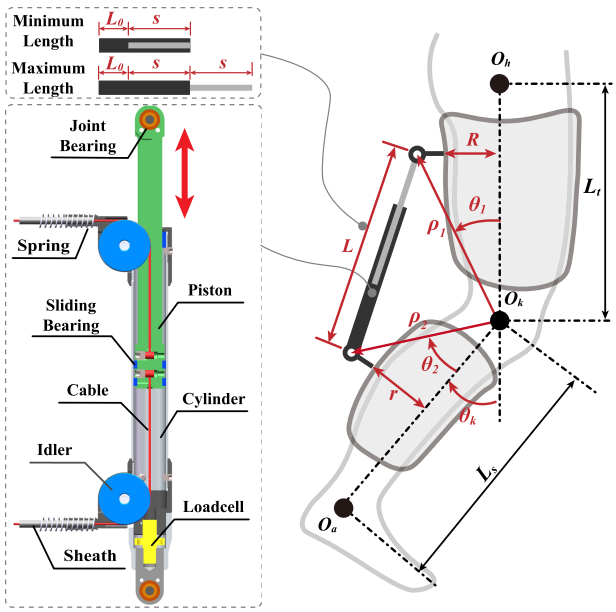

Fig. 2. Wearable component design. It consists of the proposed cable-driven linear actuator and wearable cuffs based on the 3-D contour of the human lower limbs.

1) wearable component with linear cable-driven actuator donned on the human body; and 2) remote cable driving platform integrated with graphical user interface (GUI), cable driving unit, control hardware, sensor acquisition, and battery management behind the human body.

A. Wearable Component

1) Cable-Driven Linear Actuator: The proposed linear actuator is separated from its driving and power systems through cable transmission, as shown in Fig. 2. It has a peak force capability of 260 N and a maximum speed of 1.2 m/s. The speed margin is designed to compensate for the system elasticity due to cable and cuff deformation. Two cables are used for bidirectional motions

(push and pull) of the linear actuator, respectively. One end of the cable is fixed on the inner end of the piston and out from the holes in the periphery of the cylinder. The piston is reciprocating inside the cylinder by stretching the inner cable. The actuator length increases when pulling the upper cable, and decreases when pulling the lower cable. Here, the steel wire rope (7*19, ϕ1.5 mm, max 1000 N) is adopted to replace the Bowden cable in order to keep the strength and safety under high tension force. To measure the interaction force, a load cell (Futek Inc., USA) is mounted between the end of the cylinder and the attachment component. We designed a series of actuators with different strokes, from 110 to 170 mm and a stroke interval of 10 mm, to facilitate the variation of individual sizes. Compared to our preliminary design [27], we add idlers at the cable output point on the cylinder instead of the self-lubricating plastic bearing, which largely improves the durability of the actuator.

2) Limb Cuffs: The connection cuffs are designed to snugly fit the thigh and shank contours of individual subjects, as shown in Fig. 2. The lower limb undergoes an optical scan to extract the 3-D surfaces. The locations of the two cuffs are selected to avoid interference with the human body. We also design the hinge base on the cuff model, which is used to assemble with the linear actuator. The cuffs are 3-D printed with high-performance polyamide (nylon) material to meet the requirements of mechanical strength and toughness.

3) Wearable Sensors: Various sensors are integrated to measure human locomotion information. Two inertial measurement units (IMUs) are placed on the front of the thigh cuff and the shank cuff, respectively. Two self-developed pressure insoles are used [28], each of which contains two FlexiForce (Tekscan Inc., USA) sensors to generate heel and toe pressure signals. Kinematic information from IMUs and plantar pressures from the insoles are used to calculate the knee joint angle and gait parameters, and to detect the human motion intention including locomotion phases and modes. All signals are fed into the control system with a sampling rate of 100 Hz through the serial bus.

B. Structural Parameter Optimization

The thigh and shank cuffs are connected by the cable-driven linear actuator, each end of which is hinged to the rear side of one cuff, as shown in Fig. 2. It can be observed that the locations of two hinge points will affect the reachable rotation range of the knee joint, and also affect the required length, thus the weight of the linear actuator. Therefore, this section intends to optimize the location of the linear actuator so that both aforementioned concerns are addressed.

The locations of the two hinge points are represented by a quasi-polar system, as shown in Fig. 2. The upper hinge point is described by its distance to the knee joint rotation center O_k, denoted as ρ_1, and a deviation angle from the thigh central axis $\overline{O_kO_h}$, denoted as θ_1. Similarly, the lower hinge point is determined by its distance to the knee joint rotation center O_k, denoted as ρ_2, and a deviation angle from the shank central axis $\overline{O_kO_a}$, denoted as θ_2. The linear actuator is composed of the static cylinder part and the moving piston part. Assuming the intrinsic length of the actuator to be L_0 and the stroke length to be s, the distance between the two hinge points can vary from $L_0 + s$ to $L_0 + 2\,s$, as shown in Fig. 2.

The rotation range of knee joint is characterized by the boundaries of knee angle θ_k, defined as the angle between the thigh and shank central axes, as shown in Fig. 2. It can be observed that θ_k obtains its minimal value either when the linear actuator reaches its maximum length before standing still, s.t. the thigh axis coincides with the shank axis, or when standing still, s.t. θ_k reaches 0. However, to guarantee normal operation, the linear actuator has to be designed so that $\theta_k = 0$ is reachable, which requires

$$L_0 + 2\,s \geq \rho_1 \cos\theta_1 + \rho_2 \cos\theta_2. \tag{1}$$

For practical concerns, the hinge points should not exceed the thigh and shank range, denoted as

$$\begin{cases} \rho_1 \cos\theta_1 \leq L_t \\ \rho_2 \cos\theta_2 \leq L_s. \end{cases} \tag{2}$$

The hinge points should also circumvent interventions with the cuffs, denoted as

$$\begin{cases} \rho_1 \sin\theta_1 \geq R \\ \rho_2 \sin\theta_2 \geq r \end{cases} \tag{3}$$

where R and r refer to the maximum radii of thigh and shank cuffs, respectively.

As condition (1) guarantees the minimum reachable knee angle to be 0, the rotation range of the knee exoskeleton is solely dependent on the maximum reachable knee angle θ_k^M, which is obtained when the linear actuator is at its minimum length $L_0 + s$, and can be calculated by the Cosine law

$$\theta_k^M = \pi - \theta_1 - \theta_2 - \arccos \frac{\rho_1^2 + \rho_2^2 - (L_0 + s)^2}{2\rho_1\rho_2}. \tag{4}$$

Therefore, the selection of parameters should maximize the maximum reachable knee angle θ_k^M, while minimizing the actuator weight. When the actuator weight is sized by the relative length of the stroke with respect to the actuator's intrinsic length, the cost function can be designed as

$$J = \omega_1 \theta_k^M - \omega_2 \frac{s}{L_0} \tag{5}$$

where ω_1 and ω_2 are the tuning weights for rotation range and actuator weight, respectively, and add up to 1.

Therefore, the optimal locations of hinge points and the corresponding selected stroke length can be calculated by

$$(\rho_1^*, \theta_1^*, \rho_2^*, \theta_2^*, s^*) = \arg\max J \tag{6}$$

subject to the constraints (1)–(3) and the parameter selection ranges are

$$\begin{aligned} &\rho_1, \rho_2, \theta_1, \theta_2, s \geq 0, \\ &\theta_1 + \theta_2 \leq \pi. \end{aligned} \tag{7}$$

The optimization is implemented by the Matlab Optimization Toolbox (Mathworks Inc., USA), with the selection of parameters as $\omega_1 = 0.8$, $\omega_2 = 0.2$, $R = 92.3$ mm, $r = 65.3$ mm, $L_t = 490$ mm, and $L_s = 380$ mm. The resulting optimal solutions are $\rho_1^* = 343.7$ mm, $\theta_1^* = 0.40$ rd, $\rho_2^* = 103.6$ mm, $\theta_2^* = 0.44$ rd, and $s^* = 169.1$ mm.

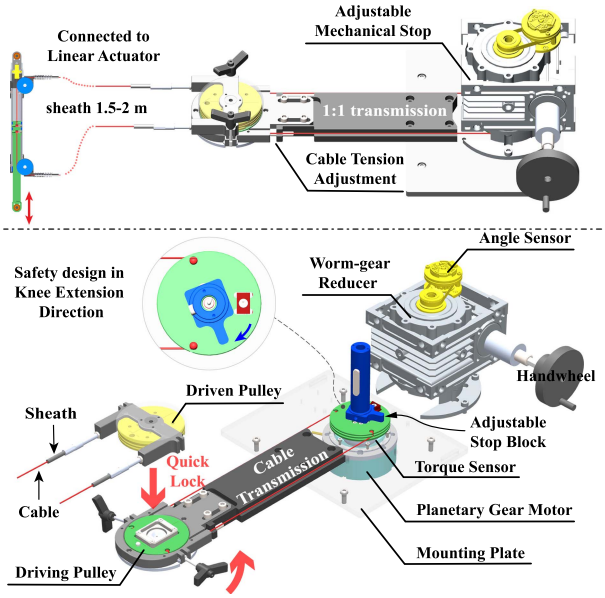

Fig. 3. Cable driving unit design. This unit is installed inside the driving platform. A quick lock between the driving pulley and the driven pulley is designed for separating the wearable component from the driving platform easily and quickly. The adjustable mechanical stop is designed for safety problems due to knee hyperextension.

C. Remote Cable Driving Platform

In the proposed exoskeleton system, remote driving is adopted to reduce the exoskeleton weight and structure size on the human limbs. A remote cable driving platform is designed for its realization, as shown in Fig. 1. Inside the platform, a dual-direction cable driving unit is designed to drive the linear actuator in the lengthening/shortening directions, as shown in Fig. 3. The cable spool is driven by a customized dc brushless motor integrated with a planetary gear reducer, with a rated torque of 10 Nm (peak 20 Nm) and a continuous speed of 300 r/min. One uniaxial torque sensor with a capacity of 50 Nm (Sunrise Instruments Co., Ltd.) is mounted between the output flange and the cable spool to measure the output torque. An inline multiturn absolute rotary encoder with 18 b/turn (Heidenhain Corp., GER) is installed at the end of the motor for speed and position measurements. A 76.5-mm diameter cable pulley is installed on the output side of the gearbox. The pulley groove is designed to be able to wrap the cable around the pulley which is limited by a two-side fixed mechanical stop (free 315°), allowing a maximum of 207 mm of cable travel.

a) Dismountable driving pulley structure: To achieve easy wearing and switching, the driving pulley structure is designed to be dismountable, as shown in Fig. 3. The cable spool is located in front of the cable driving unit, pulled by the motor behind it. A quick lock between the driving pulley and the driven pulley is designed to separate the wearable component from the driving platform. If the wear component cannot be dismounted from the remote diving platform, the donning process and space will be limited by the driving platform. More importantly, the wearable component is customized based on individual information, which needs to be realized through the quick lock.

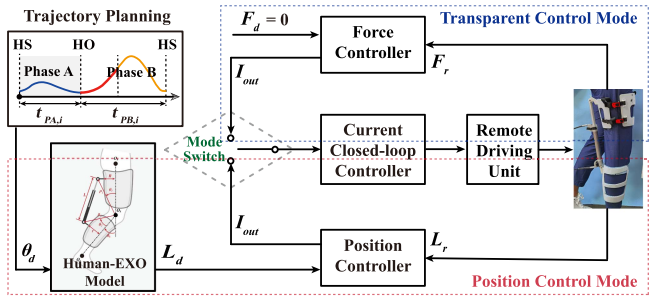

Fig. 4. Block diagram of the control system. Part 1: Transparent control is used in the process of human-exoskeleton modeling. Part 2: Position control is used for joint angle trajectory tracking in the gait intervention.

b) Adjustable mechanical stop: Human safety concern is always the first priority for the design of rehabilitation devices, especially with active intervention. For knee joints, preventing hyperextension is highly necessary. In our design, apart from the safety protection added in the control system, a continuously adjustable mechanical stop is designed to constrain the actuator motions where the self-locking property of the worm shaft and worm gear transmission is applied. For the used worm-gear reducer, the input is the worm shaft and the output is the worm gear. The stop block is installed on the worm gear through an output shaft (blue shaft in Fig. 3). We operate the worm shaft through the handwheel on the side of the actuation cabinet to continuously and precisely adjust the position of the mechanical stop. An absolute encoder (Heidenhain Corp., GER) is installed to measure the position of the worm gear, which is presented on the GUI.

III. Control System

To realize gait intervention, a control system is proposed in this section for the planning and tracking of knee joint trajectories, as shown in Fig. 4. As the proposed design circumvents the robotic knee joint, a human-exoskeleton model is required to describe the relationship between the human knee joint angle and the length of the cable-driven linear actuator. The controller contains two different modes (position control mode and transparent control mode), which play different roles during the operations. The position control mode is used to track the joint trajectory during gait intervention. The transparent control mode based on zero-force control is used to obtain the human-exoskeleton model, as it generates the required low resistance of the exoskeleton for the modeling process. The obtained human-exoskeleton model is then applied as a part of the position control mode for gait intervention. In other words, those two control modes are not alternatives.

A. Human-Exoskeleton Kinematic Model

The joint-free structure of the proposed exoskeleton requires a human-exoskeleton kinematic model to build the relationship between the human joint angle and linear actuator length. It has been verified in our previous work [27] that such a relationship

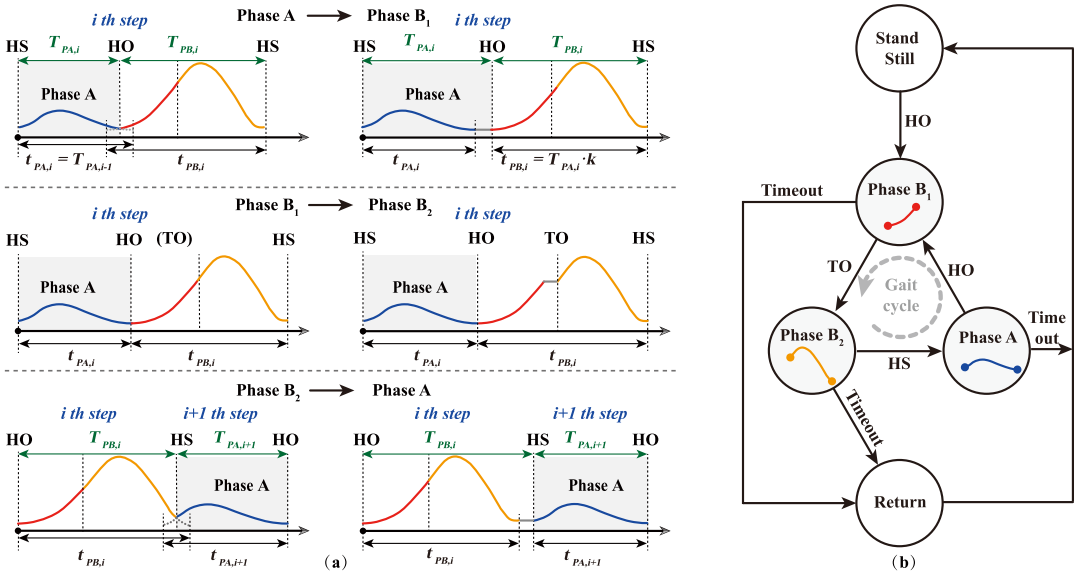

Fig. 5. (a) Trajectory planning when gait events are detected in advance or delayed, including heel strike (HS), heel off (HO), and toe off (TO). (b) Finite state machine (FSM) diagram. It shows how to switch in five predefined states which consider starting from standing, normal gait cycle and abnormal situation.

can be fitted by a quadratic structure

$$L = a\theta_k^2 + b\,\theta_k + c \tag{8}$$

where L refers to the linear actuator length, and a, b, and c are fitting coefficients.

In contrast with [27], this article collects the fittings data from the sensory system under the transparent control mode; thus it avoids the requirements of a motion capture system for practical concerns. During the modeling process, the interaction force is measured by the loadcell sensor installed on the cable-driven linear actuator, and the reference force of the controller is set to zero. Multiple θ_k along the operation range and their corresponding actuator lengths are recorded, and the coefficients in (8) are then fitted through a least-square method.

B. Trajectory Tracking-Based Gait Intervention Strategy

This section presents a gait intervention strategy of the proposed exoskeleton, which can be used to correct the abnormal walking pattern during lower limb rehabilitation. The strategy is demonstrated in Figs. 4 and 5(b), which consists of the generation and tracking of joint angle trajectories, finite state machine for gait phase and mode transition, and adaptation of cycle duration and phase proportions.

1) Position Controller: The position controller convert the desired joint angle trajectory into the reference of linear cable-driven actuator length through the fitted human-exoskeleton kinematic model. A high-bandwidth tracking controller is applied to achieve precise control of the linear actuator length, thus the knee joint angle.

2) Trajectory Generation: The desired joint trajectory is generated by the connection of multiple sectional curves. The knee joint angle trajectory curve of a gait cycle [0% is defined as heel strike (HS)] is divided into two phases: 1) Phase A; and 2) Phase B. The gait event heel off (HO) is the transition point from Phase A to Phase B. Phase B is further divided into Phase B_1 and Phase B_2, mainly due to safety considerations as large movements in Phase B_2 could cause falling. The gait event toe off (TO) is the transition point from Phase B_1 to Phase B_2. Actually, Phase A and Phase B_1 combines to form the stance phase and Phase B_2 is the swing phase of a gait cycle.

Generally, it is difficult to detect the exact moment for notable gait events such as HS, HO, or TO. Therefore, we need to consider how to handle the juncture between two adjacent trajectory curves smoothly and continuously. We displayed six situations in Fig. 5(a). For Phase A to Phase B_1, when HO happens in advance, Phase A stops immediately, and Phase B_1 starts with the angle which is the value at the stop moment of Phase A. When HO is delayed, the angle in Phase A maintains its value until HO happens. For Phase B_1 to Phase B_2, if the TO happens before Phase B_1 finished, Phase B will continue without interruption. On the other hand, the actuator will stop at the end of Phase B_1 till TO happens. For Phase B_2 to Phase A, when next HS happens in advance, Phase B_2 stops immediately, and Phase A of the next gait cycle starts with the angle which is the value at the stop moment of Phase B_2. When HS is delayed, Phase B_2 maintains until HS of the next step occurs.

3) Finite State Machine: Finite state machine (FSM) is used in the gait controller for gait phase and locomotion mode transitions. Fig. 5(b) illustrates the FSM diagram which includes five states: *{Return to initial state, Stand still, Phase A, Phase B_1, Phase B_2}*. Gait event detections are based on the pressure information of force insole (P_{heel} and P_{toe}) and adopts threshold method. th_1 and th_2 are predefined pressure threshold of heel and toe, respectively. For example, $P_{\text{heel}} < th_1$ is HO and otherwise HS. The conditions for states transition are displayed in Table I. The cyclical transitions between states *{Phase A, Phase B_1, Phase B_2}* make up a complete walking gait. In addition,

TABLE I
CONDITIONS OF FINITE STATE MACHINE

State Transition	Conditions
Phase A→Phase B1	Heel Off ($P_{\text{heel}}<th_1$)
Phase B1→Phase B2	Toe Off ($P_{\text{heel}}<th_1$, $P_{\text{toe}}<th_2$)
Phase B2→Phase A	Heel Strike ($P_{\text{heel}}>th_1$, $P_{\text{toe}}<th_2$)
Stand still→Phase B1	Heel Off ($P_{\text{heel}}<th_1$)
Others	Timeout

the gait starts when HO happens in the state *{Stand still}*. The exoskeleton will slowly extend to initial state *{Return to initial state}*, and then, wearer remains standing *{Stand still}* when the detection condition is timeout.

4) Phase Proportion and Cycle Duration Adaptation: Variations of subject walking speed and characteristics require adaptations of the exoskeleton on cycle duration and phase proportion to comply better with human motions. Define t as the duration notation, e.g., $t_{PA,i}$, the desired duration of Phase A in the ith step. T represents the actual duration while the subject is walking. Phases A and B duration are represented by T_{PA} and T_{PB}, respectively. We assume that $t_{PA,i}$ for the current step is equal to the measured value of the last phase as

$$t_{PA,i} = T_{PA,i-1}. \tag{9}$$

$t_{PB,i}$ for the current step is based on the measured value of Phase A in the last step as

$$t_{PB,i} = T_{PA,i} \cdot K \tag{10}$$

where the ratio K is given by

$$K = \frac{1-P}{P}. \tag{11}$$

P is calculated from the last five gait cycles, with a default value of 32% [29]. Therefore, the default K is 2.125 according to (11). According to the calculated phase duration for the current step, the trajectory is interpolated again and updated into the position controller in real time.

Control parameters limits are set carefully. If the calculated $t_{PA,i}$ and $t_{PB,i}$ are very small, the linear actuator will run fast. On the contrary, the system will run slowly. Therefore, $t_{PA,i}$ and $t_{PB,i}$ is set to vary in the range $[P \cdot CD_{\min}, P \cdot CD_{\max}]$ and $[(1-P) \cdot CD_{\min}, (1-P) \cdot CD_{\max}]$, respectively. P is defined as the proportion of Phase A in a gait cycle and CD represents the cycle duration in the interval ($CD_{\min}$ and $CD_{\max}$). Therefore, if the value of T_{PA} and T_{PB} is outside the range, the system will be switched to a safe mode where the exoskeleton recovers to 0° gradually and the subject stands upright slowly.

IV. EXPERIMENTAL PROTOCOL

A. Transparent Control Performance Analysis

1) Leg Swing Test: The subject was asked to stand on his left leg and swing his right leg (exoskeleton side) with gradually increasing frequency under two conditions: Transparent control OFF(power off) and transparent control ON. Before the experiment, the subject was allowed to make attempts with the exoskeleton to get familiar with the test task. The task consists of about fifteen cycles and a cycle is defined as the maximum knee extension angle to the maximum knee flexion and then back to the initial states. The knee angle, angular velocity, and interaction force were recorded to analyze the transparent effect. A healthy subject (20 years old, height 175 cm, and weight 61 kg) was involved in this task. He provided informed written consent before being involved in the experiment. All the following experiments in this section have been approved by the Local Ethics Committee of Peking University.

2) Walking Test: Except the leg swing test, we also observed its performance during walking. The subject was asked to walk on the treadmill at a speed of 0.8 m/s for 3 min while wearing the exoskeleton on his right leg in transparent control mode. The knee angle and the interaction force were recorded and normalized by gait cycle (from heel strike to next heel strike).

B. Position Control Performance

Position trajectory tracking experiments with and without load were conducted. One end of the proposed linear cable-driven actuator is fixed on a customized framework along the gravity direction. In the load test, the other end of the actuator hangs a 20-kg weight. The desired trajectory is a 1-Hz sine curve with 31-mm amplitude. The desired linear actuator length is from 260 mm to 326 mm, and the maximum speed can reach 207 mm/s. Trajectory control test with and without loading lasted 10 s (10 cycles), respectively. The root mean square error (RMSE) and maximum error are calculated in MATLAB to evaluate the control performance.

C. Mechanical Efficiency Analysis

The mechanical efficiency of the proposed exoskeleton with a linear cable-driven actuator and a long-distance cable transmission is an interesting question. In our exoskeleton system, the distance from the motor output end to the linear actuator is approximately 2 m, and the linear actuator design is different from the common design based on the lead screw or ball screw structure in wearable robots.

A test bench setup (shown in the Result section) was designed to experimentally analyze the mechanical efficiency of the whole mechanical transmission structure from the motor output end to the linear actuator output end. The linear cable-driven actuator is installed in the framework and can lift the load along the gravity direction, the loadcell can measure the force in real time, and the displacement transducer can measure the position in real time to calculate the linear velocity.

The power consumed (P_{input}) can be calculated by the product of the motor output torque (torque sensor shown in Fig. 3) and angular velocity (motor encoder). The power delivered (P_{output}) can be calculated by the product of output force and linear velocity. The mechanical efficiency is

$$\eta = \frac{P_{\text{output}}}{P_{\text{input}}} \times 100\%. \tag{12}$$

D. Impact of Wearing Exoskeleton on Normal Gait Kinematics

In order to evaluate the adverse impact of the proposed exoskeleton on the normal gait (e.g., mechanical structure, wearable weight, and gait control strategy), we design comparative experiments which include three conditions and analyze the gait symmetry of wearers. Six healthy male subjects participated in this experiment. Their information is 23.7±4.0 years old, height 176.8±10.0 cm, and weight 69.3±5.9 kg. They provided informed written consent before being involved in the study.

In Condition I, the subject walks on the treadmill without the exoskeleton. In Condition II, the subject walks with the wearable component but without the remote driving platform. It means that the linear actuator of the wearable component is not connected to the motor and can move freely with only itself friction force. In Condition III, the subject walks in trajectory control mode. The desired trajectory was set according to his gait parameters which are recorded and calculated from kinematic data in Condition I.

Each subject walked on the treadmill at 0.8 m/s under three conditions, and each lasted for three minutes. The kinematic data are collected using the optical motion capture system (Motion Analysis, USA), and the ground reaction force (GRF) is recorded simultaneously using a treadmill with force plates (h/p/cosmos, Germany). The knee angle was calculated using the Helen-Hayes lower limb model. The symmetry index (SI) is calculated by

$$\mathrm{SI} = \left|\frac{V_L - V_R}{0.5 \times (V_L + V_R)}\right| \times 100\% \tag{13}$$

where the V_L and V_R stand for gait variables recorded from the left and right sides, respectively. The closer SI value is to zero, the more symmetric the gait parameter is. We choose ten variables for symmetry evaluation, as listed in Table II.

E. Gait Intervention Using Exoskeleton

A series of experiments are designed as shown in Fig. 6. First, a preexperiment is conducted where the subject walks with the wearable component but without the remote driving platform, which means that the linear actuator can be moved freely. After this process, the personalized gait parameters (Baseline) were calculated from the kinematic data. Then, the subject walks in trajectory control mode with the baseline gait parameters. Finally, it follows two kinds of gait intervention experiments (A and B). The human joint angle curve of the gait cycle as a time-domain signal has two types of characteristics, one of which is angle value, e.g., peak value, valley value, and the other of which is time, e.g., phase proportion, cycle duration, etc. Therefore, we selected two parameters, which are peak angle and Phase A proportion. We tried to intervene the gait through giving different peak angles and designed Intervention A experiment. The subject was asked to walk under the trajectory control mode with adjusted peak angle parameters (θ_p+Δ, θ_p-Δ). We also tried to intervene the gait through giving different phase percentages and designed Intervention B experiment. The subject was asked

TABLE II
GAIT SYMMETRY INDEXES (SI) FOR SIX SUBJECTS UNDER THREE WALKING CONDITIONS (I, II, AND III)

No.	Con	θ_p	t_{θ_p}	P_{ST}	CD	F_1	t_1	F_2	t_2	F_3	t_3
S1	I	3.9	1.2	1	0.1	1.0	2.5	1.1	4.2	2.6	1.4
	II	5.0	2.6	0.4	0.1	1.4	13.5	0.3	2.8	0.1	4.7
	III	2.3	2.9	1.6	0.1	2.5	12.7	1.4	6.6	2.9	3.4
S2	I	0.2	0.4	2.8	0.1	1.8	0.4	1.1	12.9	0.9	1.9
	II	13.7	1.0	5.4	0.6	1.5	4.5	1.5	10.4	1.7	5.6
	III	14.0	0.4	1.8	0.1	1.4	4.5	0.5	4.2	1.0	0.8
S3	I	5.3	0.0	1.6	0.0	0.2	0.0	0.3	3.7	0.9	0.6
	II	4.3	0.6	0.3	0.0	0.0	3.0	1.0	5.8	2.0	0.8
	III	8.4	0.3	1.9	0.1	0.8	4.8	0.3	5.4	1.5	5.6
S4	I	5.4	0.7	0.3	1.9	0.3	11.5	0.1	5.1	0.3	1.0
	II	5.5	1.3	1.3	1.1	0.9	6.3	0.7	6.0	2.5	1.6
	III	7.7	0.1	2.9	2.2	2.8	4.7	1.6	1.7	0.2	3.5
S5	I	2.3	1.7	2.7	2.3	1.8	10.6	2.4	2.4	0.3	7.6
	II	2.2	1.3	2.4	3.5	0.9	13.3	0.4	0.6	2.5	5.1
	III	2.9	0.1	2.6	1.1	1.2	8.4	1.0	2.5	2.6	0.0
S6	I	4.3	2.9	2.8	2.6	2.8	4.8	0.8	2.8	0.1	3.2
	II	1.0	6.0	4.8	1.8	0.2	1.9	0.9	1.7	1.9	18.9
	III	8.8	8.1	4.1	2.3	0.2	1.9	0.7	1.8	1.9	2.9
Ave	I	3.6	1.1	1.9	1.2	1.3	5.0	1.0	5.2	0.9	2.6
	II	5.3	2.1	2.4	1.2	0.8	7.1	0.8	4.5	1.8	6.1
	III	7.4	2.0	2.5	1.0	1.5	6.2	0.9	3.7	1.7	2.7

θ_p is the peak angle in the gait cycle and t_{θ_p} is the corresponding time; R_{ST} is the proportion of stance phase; CD is gait cycle duration; F_{1-3} are the first peak force, the valley force, and the second peak force of GRF curve and t_{1-3} are the corresponding moment, respectively.

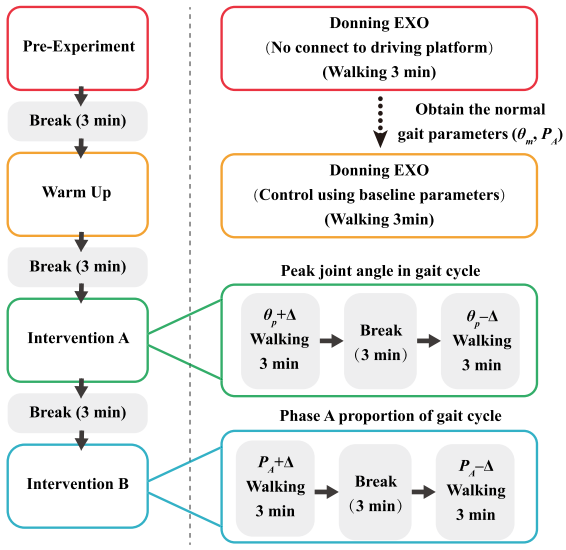

Fig. 6. Gait intervention experiment protocol. Firstly, pre-experiment: donning wearable component but no connecting to the remote driving platform. Then, warm up: Donning exoskeleton and walking with baseline parameter. Finally, two gait interventions (A and B) using the proposed exoskeleton. Interventions A: Adjustment of the peak angle parameter in the gait cycle. Interventions B: Adjustment of Phase A proportion of gait cycle.

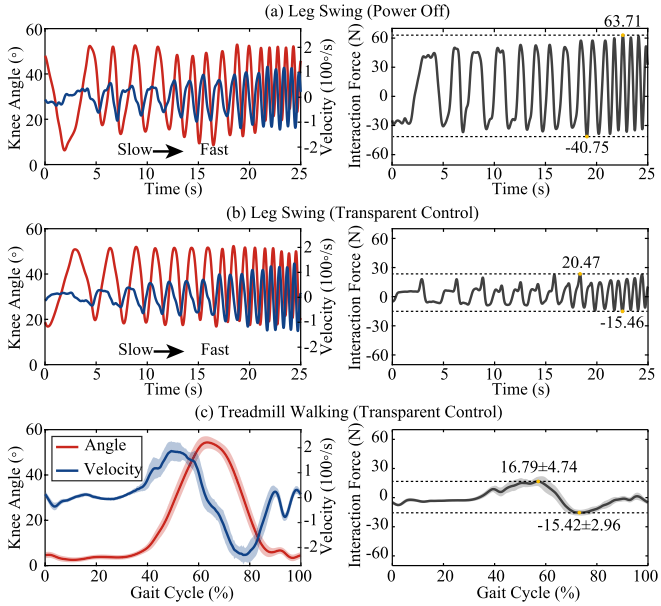

Fig. 7. Transparent control. (a) and (b) The subject stands on his left leg and swings his right leg with exoskeleton under power off and transparent mode, respectively. (c) The subject with the exoskeleton under transparent mode walks on the treadmill.

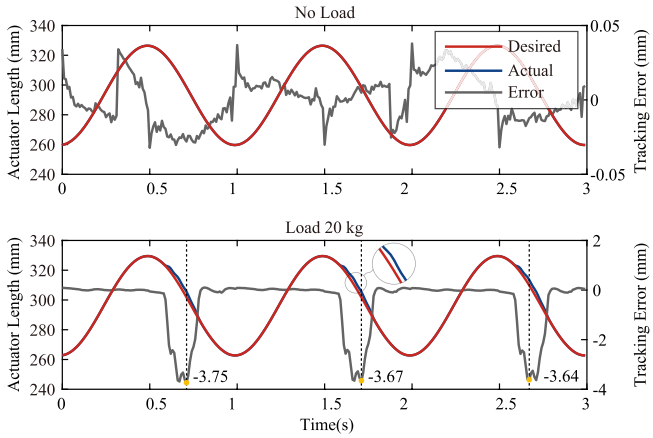

Fig. 8. Trajectory control. The top and bottom figures show the tracking performance without load and with a 20-kg load, respectively.

to walk under the trajectory control mode with adjusted Phase A proportion parameter (P_A+Δ, P_A-Δ). We set a three minutes break between each intervention group. Six subjects participated in the intervention experiments. Their information is 22.8±1.7 years old, height 178.7±6.4 cm, and weight 71.3±6.1 kg. They provided informed written consent before being involved in the study. For the gait intervention effect evaluation, we calculated mean absolute error (MAE) by

$$\text{MAE} = \frac{\sum_{i=1}^{n} |\text{desired}_i - \text{actual}_i|}{n} \tag{14}$$

F. Verification of Support Ability

This experiment was designed to verify the supporting ability of our Hybrid-KEX system. A healthy subject (24 years old, height 170 cm, weight 73 kg) participated in this experiment. He was asked to do squat-to-stand and squat-to-stand transitions repeatedly. The exoskeleton works in trajectory mode during the test. The loadcell sensor on the actuator records the output push force, which is regarded as the support force provided by the exoskeleton. The knee torque is calculated by the product of the perpendicular line length from the knee joint rotation center to the axis of the linear actuator and the output force of the linear actuator.

V. Results

A. Transparent Control

In Fig. 7(a), the knee exoskeleton under power OFFcondition is driven by the human knee, the knee angle ranges from 9.6° to 52.4°, the knee angular velocity reaches a maximum of about 129.5 °/s, and the interaction force ranges from –40.75 N to 63.71 N. It indicates the system's backdrivable performance. In Fig. 7(b), when entering the transparent control mode, the joint motion range keeps similar (from 16.8° to 52.3°), the knee angular velocity reaches a maximum of 135.4 °/s, and the interaction force ranges from –15.46 N to 23.47 N. Those results indicate that the interaction force during voluntary leg swing is significantly lower when transparent control is on, and the swing velocity increases due to the transparent effect. In Fig. 7(c), when a subject was walking on the treadmill under 0.8 m/s speed, the knee angular velocity can reach 227.2 °/s which increases about 70% and the interaction force ranges from –15.42 N to 16.79 N whose effect is similar compared with the leg swing test. The results indicate that the transparent mode can work well in actual walking.

B. Trajectory Control

Position trajectory tracking performance is shown in Fig. 8. The desired trajectory of the linear cable-driven actuator is a 1 Hz sine signal from 260 to 326 mm. For the no-load test, the RMSE value is 0.02 mm, and the maximum error (absolute value) is 0.04 mm. And for the load test, the piston of the actuator hangs a 20-kg load, and the load force is nearly 200 N due to gravity. The RMSE value is 1.20 mm, and the maximum error (absolute value) is 3.75 mm. The maximum tracking error happens after the direction changes from shortening to lengthening. Those results indicate that the exoskeleton can perform fine trajectory tracking for further gait intervention.

C. Mechanical Efficiency

In the test experiment, the motor is controlled to keep a constant angular speed, the load (about 11.27 kg) is lifted about 120 mm, and the linear velocity is about 207 mm/s. We repeated the lifting process 15 times and calculated the input/output power and efficiency. The efficiency is from a minimum of 72.9% to a maximum of 83.8%, and the average is 76.6%±2.9%, as shown in Fig. 9. We also made a comparison with other linear

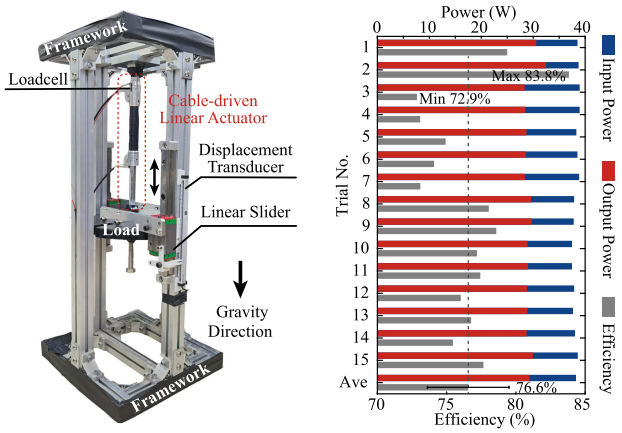

Fig. 9. Mechanical efficiency analysis. The left figure is the test bench setup, and the right one is the testing results.

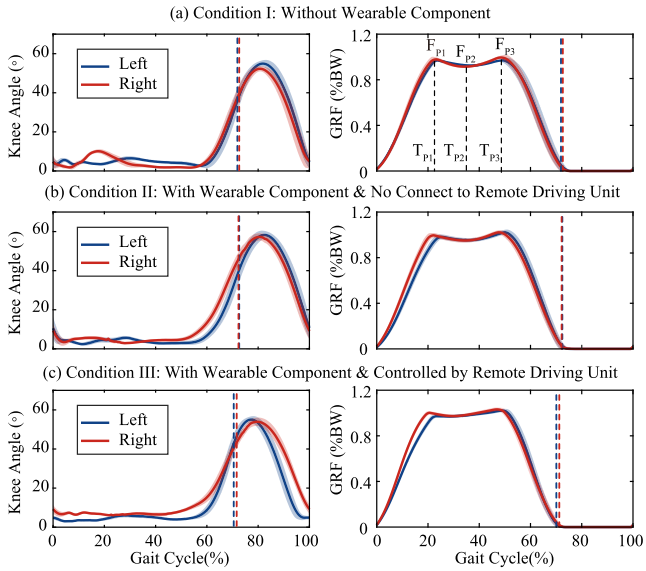

Fig. 10. Symmetric result of a representative subject. The left and right columns are knee joint angle and GRF normalized to the gait cycle, respectively. Vertical dashed line: transition of stance to swing phase.

motion commercial products (Thomson Industries, Inc). The mechanical efficiency of the lead screw is from 37% to 82% and the ball screw is 88%±5%. In conclusion, the mechanical efficiency of the whole transmission in our system is below the ball screw and close to the lead screw with a large lead (≥ 8 mm).

D. Impact of Exoskeleton on Normal Gait Kinematics

Fig. 10 demonstrates the bilateral knee angle and GRF of a representative subject. The asymmetry indexes for all the subjects were calculated and listed in Table II. The average value of the three conditions are 2.4±1.7%, 3.2±2.3%, and 3.0±2.2%. A paired t-test with a significant level $\alpha = 0.05$ between any two conditions is conducted to test the statistical significance. Comparing the results between Condition I and Condition II, it is found that the wearable component weight and mechanical structure have minimal impact on gait symmetry (SI increases by 0.6%, $p = 0.068$). It is concluded that the trajectory control strategy using personalized parameters works well by comparing the results between Condition II and Condition III ($p = 0.551$) and between Condition I and Condition III ($p = 0.209$).

TABLE III
FEATURE COMPARISON OF THREE TYPES OF EXOSKELETONS

Feature	Rigid	Soft	Hybrid
Bulkiness	Bulky	Low profile and light weight	Low profile and light weight
Joint alignment	Require complex mechanisms	Easily achieved	Easily achieved
Impact on normal gait kinematics	Usually alter kinematics	Little to no effect	Little to no effect
Joint assistance	Bidirectional	Unidirectional	Bidirectional
Body support	Yes	No	Yes
Mechanical stop	Yes	No	Yes

E. Gait Intervention Using Exoskeleton

For the gait intervention of the peak value of the joint angle curve, we set two groups (θ_p+Δ and θ_p-Δ) based on the baseline curve where Δ is 4°. Fig. 11(a) presents the result of a representative subject (Subject 1). We can find that the exoskeleton with the proposed gait intervention strategy can increase or decrease the peak angle of the wearer's gait. We also calculated all subjects' results and the MAE is 1.42±0.59°, as shown in Fig. 11(b) and (c). We also set two groups (P_A+Δ and P_A-Δ) based on the baseline curve where Δ is 2 for the gait intervention of Phase A proportion. The result of a representative subject (Subject 1) is shown in Fig. 11(d) and the exoskeleton with gait intervention strategy can change the gait phase proportion. All subjects' results are shown in Fig. 11(e) and (f) and the MAE is 0.88±0.34%.

F. Support for Squat-to-Stand Transition

As shown in Fig. 12, the knee angle curve indicates that the subject is from stand to squat and then back to stand. The knee flexes to approximately 30° and keeps for about 2 s. The torque acting on the human body from the exoskeleton reaches more than 17.5 Nm and sustains during the whole squat state. The result indicates that the proposed rigid-soft Hybrid-KEX system can provide effective assistance and supporting ability.

VI. DISCUSSION

A. Advantages of Soft-Rigid Hybrid Structure

The proposed Hybrid-KEX design for gait training and intervention gathers the advantages of soft exoskeletons, e.g., lightweight, small inertia, and minimal impact on normal walking, while being able to perform bidirectional joint motion intervention safely and to provide effective supporting ability as the rigid exoskeleton. Feature comparison of three types of exoskeletons is listed in Table III.

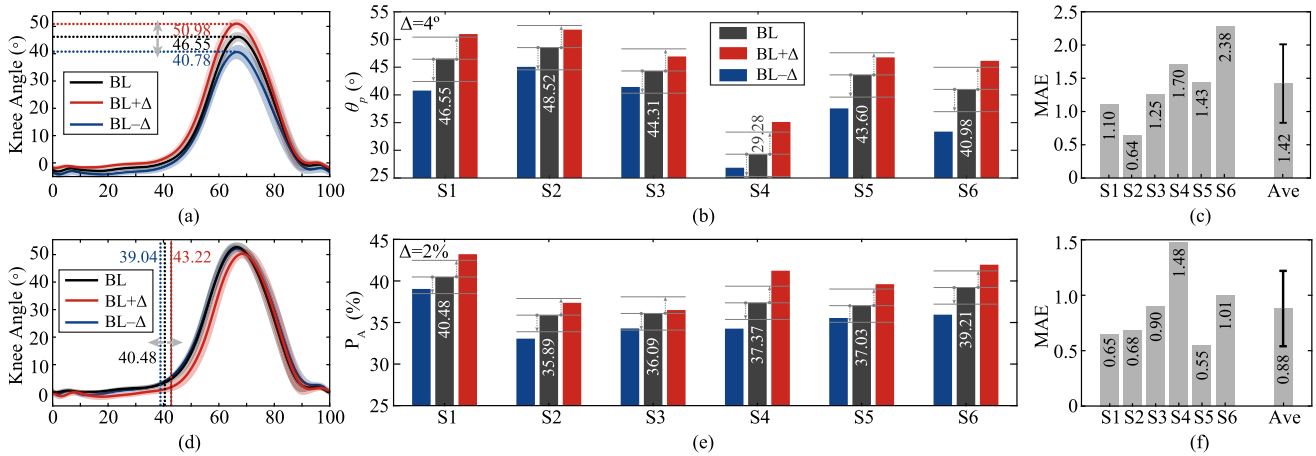

Fig. 11. Gait intervention analysis. (a)–(c) Adjustments of peak joint angle (Baseline (BL)±Δ). (d)–(f) Adjustments of Phase A proportion (BL±Δ). (a) and (b) Normalized joint angle profiles of a representative subject (S1) with gait intervention. (b) and (c) Peak knee angle adjustment for all subjects (S1–S6). (e) and (f) Phase A proportion adjustment for all subjects (S1-S6).

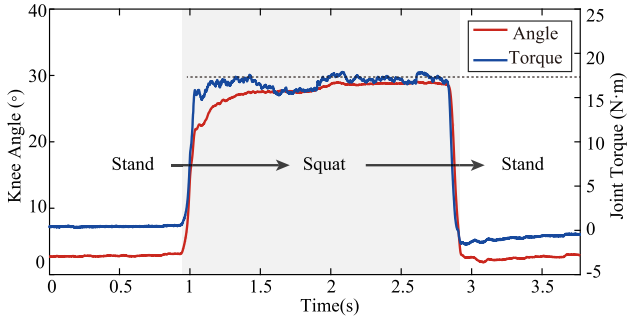

Fig. 12. Body support using exoskeleton during squat-to-stand transition.

1) Exoskeleton Joint-Free Design: The robotic joint is a key feature of rigid exoskeletons [5]. The anatomical and exoskeleton joints are not perfectly aligned, which can create high interaction forces [15], alter the wearer's natural gait, and/or create discomfort at the interfaces [23]. The self-aligning mechanism tries to solve the problem [16], [17], [18], [19], [20], but adds extra weight, e.g., 190 g [16]. In addition, those designs only work on the sagittal plane and/or the frontal plane and cannot fully compensate for the misalignment. Therefore, soft exoskeletons with the joint-free design were proposed [23], [24], [26] to avoid the misalignment completely.

2) Lightweight Wearable Component: Apart from joint misalignment, the bulkiness of wearable component also brings a negative impact on normal gait kinematics, where soft exoskeletons generally have an innate advantage compared to rigid ones. In the recent five years, the weight of representative rigid exoskeletons varies from 3.6 kg to 4.1 kg [16], [11]. Even without the battery module, the weight of existing rigid exoskeletons can reach a minimum of 2.1 kg [14] (other works include 2.8 kg [12], 2.7 kg [10], 2.5 kg [8]). The wearable component of our proposed system Hybrid-KEX reaches a weight of 1.2 kg, which is much smaller compared with the existing rigid systems, and comparable with the state-of-the-art soft exoskeleton [23] (1.14 kg). It should be admitted that the cable-driven actuator has a natural advantage in weight, so that the weight comparison may not be fair. However, this comparison provides a weight reference in the sense of functionality, as our proposed system addresses the key advantages of the rigid exoskeleton, especially the support ability.

3) Minimal Impact on Normal Gait Kinematics: Few exoskeletons have actually evaluated whether they truly avoid unnaturally constraining or otherwise impacting the wearer's gait [23]. The knee extension exosuit study has done such validation by comparing the mean angle profiles of walking without wearing the exosuit with wearing the exosuit in the unpowered mode [23]. Similar analysis can also be found for MyoSuit [24]. In this article, comprehensive experiments under three conditions (normal walking without the exoskeleton, wearing the exoskeleton without the remote driving unit, and exoskeleton control with baseline parameters) are conducted to evaluate the gait symmetry (angle and GRF profiles), thus the impact level on normal walking.

4) Safety Design for Knee Hyperextension: Rigid exoskeletons can easily constrain the joint range for active operation by the integration of a mechanical stop. However, such component becomes challenging for soft exoskeletons due to their joint-free characteristics. Lack of constraints in joint operation range may cause hyperextension, and further injury of the knee joint. Previous work addresses this issue by setting limitations in the controller [23], of which the reliability may vary due to uncertainties in sensing and control. In our Hybrid-KEX system, apart from the safety protection in the controller, an adjustable mechanical stop based on the worm and worm gear mechanism, and its self-locking property is designed to avoid the potential for knee joint hyperextension, similar to the rigid configurations.

5) Gait Intervention and Support Ability: Rigid exoskeletons can provide bidirectional joint torque but soft ones generally provide unidirectional torque (knee extension) as cable only

works in the tensile direction [23], [24], [26]. The proposed Hybrid-KEX can drive bidirectional joint movements like rigid ones, which has been verified in the gait intervention experiments. Such interventions are difficult to realize on conventional soft knee exoskeletons. We also carried out the squat-to-stand experiment to show that the proposed exoskeleton system can provide effective supporting ability like the rigid exoskeletons.

B. Limitations and Future Work

In this article, only healthy subjects were involved to verify the feasibility and performance of the proposed Hybird-KEX system. Our long-term goal is to help restore knee function during walking for patients with neuromuscular injuries and disorders. Future work will include improvements of the human–exoskeleton interface, and the gait controller and verification of its effectiveness in clinical rehabilitation.

VII. Conclusion

In this article, a rigid-soft hybrid knee exoskeleton for gait rehabilitation is proposed. The exoskeleton is driven by the remote driving platform through a cable-sheath transmission structure. It is lightweight to wear. The joint-free design avoids the joint misalignment issue of the rigid configurations. Meanwhile, the unique structure is able to provide much more load support compared with the soft ones, and also adjustable mechanical stop structure to circumvent the potential injury from knee hyperextension. Walking experiments were performed to verify that the proposed system has minimal impact on normal gait kinematics. A gait intervention strategy is designed based on the planning and tracking of joint angle trajectories. The results from intervention experiments with desired gait parameters indicate that the proposed exoskeleton can implement quantitative gait intervention. In addition, the squat-to-stand experiment verifies the supporting ability of our exoskeleton. Therefore, the proposed Hybrid-KEX has potential applications for clinical gait rehabilitation.

Acknowledgment

The authors would like to thank T. Zhang, Y. Zhou, and G. Zhang for their contributions in prototype implementation.

References

[1] M. Xiloyannis et al., "Soft robotic suits: State of the art, core technologies, and open challenges," *IEEE Trans. Rob.*, vol. 38, no. 3, pp. 1343–1362, Jun. 2022.
[2] A. J. Young et al., "State of the art and future direction for robotic lower limb exoskeletons," *IEEE Trans. Neural Syst. Rehabil. Eng.*, vol. 25, no. 2, pp. 171–182, Feb. 2017.
[3] L. N. Awad et al., "A soft robotic exosuit improves walking in patients after stroke," *Sci. Trans. Med.*, vol. 9, no. 400, 2017, Art. no. eaai9084.
[4] A. M. Dollar and H. Herr, "Lower extremity exoskeletons and active orthoses: Challenges and state-of-the-art," *IEEE Trans. Rob.*, vol. 24, no. 1, pp. 144–158, Feb. 2008.
[5] A. T. Asbeck, S. M. M. De Rossi, I. Galiana, Y. Ding, and C. J. Walsh, "Stronger, smarter, softer: Next-generation wearable robots," *IEEE Robot. Autom. Mag.*, vol. 21, no. 4, pp. 22–33, Dec. 2014.
[6] J. J. O'connor et al., "The geometry of the knee in the sagittal plane," *Proc. Inst. Mech. Eng., Part H: J. Eng. Med.*, vol. 203, no. 4, pp. 223–233, 1989.
[7] J. Wismans et al., "A three-dimensional mathematical model of the knee-joint," *J. Biomech.*, vol. 13, no. 8, pp. 677–685, 1980.
[8] M. Sun et al., "Lightweight electrohydrostatic actuator drive solution for exoskeleton robots," *IEEE/ASME Trans. Mechatron.*, vol. 27, no. 6, pp. 4631–4642, Dec. 2022.
[9] M. Sharifi, J. K. Mehr, V. K. Mushahwar, and M. Tavakoli, "Autonomous locomotion trajectory shaping and nonlinear control for lower limb exoskeletons," *IEEE/ASME Trans. Mechatron.*, vol. 27, no. 2, pp. 645–655, Apr. 2022.
[10] D. Lee, E. C. Kwak, B. J. McLain, I. Kang, and A. J. Young, "Effects of assistance during early stance phase using a robotic knee orthosis on energetics, muscle activity, and joint mechanics during incline and decline walking," *IEEE Trans. Neural Syst. Rehabil. Eng.*, vol. 28, no. 4, pp. 914–923, Apr. 2020.
[11] M. K. Shepherd and E. J. Rouse, "Design and validation of a torque-controllable knee exoskeleton for sit-to-stand assistance," *IEEE/ASME Trans. Mechatron.*, vol. 22, no. 4, pp. 1695–1704, Aug. 2017.
[12] M. R. Tucker, C. Shirota, O. Lambercy, J. S. Sulzer, and R. Gassert, "Design and characterization of an exoskeleton for perturbing the knee during gait," *IEEE Trans. Biomed. Eng.*, vol. 64, no. 10, pp. 2331–2343, Oct. 2017.
[13] Z. F. Lerner et al., "A lower-extremity exoskeleton improves knee extension in children with crouch gait from cerebral palsy," *Sci. Trans. Med.*, vol. 9, no. 404, 2017, Art. no. eaam9145.
[14] X. Liu and Q. Wang, "Real-time locomotion mode recognition and assistive torque control for unilateral knee exoskeleton on different terrains," *IEEE/ASME Trans. Mechatron.*, vol. 25, no. 6, pp. 2722–2732, Dec. 2020.
[15] D. Zanotto, Y. Akiyama, P. Stegall, and S. K. Agrawal, "Knee joint misalignment in exoskeletons for the lower extremities: Effects on user's gait," *IEEE Trans. Robot.*, vol. 31, no. 4, pp. 978–987, Aug. 2015.
[16] S. V. Sarkisian, M. K. Ishmael, G. R. Hunt, and T. Lenzi, "Design, development, and validation of a self-aligning mechanism for high-torque powered knee exoskeletons," *IEEE Trans. Med. Rob. Bionics*, vol. 2, no. 2, pp. 248–259, May 2020.
[17] D. Wang, K. -M. Lee, J. Guo, and C. -J. Yang, "Adaptive knee joint exoskeleton based on biological geometries," *IEEE/ASME Trans. Mechatron.*, vol. 19, no. 4, pp. 1268–1278, Aug. 2014.
[18] L. Saccares, I. Sarakoglou, and N. G. Tsagarakis, "iT-Knee: An exoskeleton with ideal torque transmission interface for ergonomic power augmentation," in *Proc. IEEE/RSJ Int. Conf. Intell. Robots Syst.*, 2016, pp. 780–786.
[19] M. Yalcin et al., "AssistOn-Knee: A self-aligning knee exoskeleton," in *Proc. IEEE/RSJ Int. Conf. Intell. Robots Syst.*, 2013, pp. 996–1002.
[20] H. Zhu, C. Nesler, N. Divekar, V. Peddinti, and R. D. Gregg, "Design principles for compact, backdrivable actuation in partial-assist powered knee orthoses," *IEEE/ASME Trans. Mechatron.*, vol. 26, no. 6, pp. 3104–3115, Dec. 2021.
[21] T. Kim, M. Jeong, and K. Kong, "Bioinspired knee joint of a lower-limb exoskeleton for misalignment reduction," *IEEE/ASME Trans. Mechatron.*, vol. 27, no. 3, pp. 1223–1232, Jun. 2022.
[22] M. Xu, Z. Zhou, J. Shao, L. Ruan, and Q. Wang, "Reducing migration of knee exoskeletons with dynamic waist strap," *IEEE Trans. Med. Robot. Bionics*, vol. 4, no. 3, pp. 764–774, Aug. 2022.
[23] E. J. Park et al., "A hinge-free, non-restrictive, lightweight tethered exosuit for knee extension assistance during walking," *IEEE Trans. Med. Robot. Bionics*, vol. 2, no. 2, pp. 165–175, May 2020.
[24] K. Schmidt et al., "The myosuit: Bi-articular anti-gravity exosuit that reduces hip extensor activity in sitting transfers," *Front. Neurorobot.*, vol. 11, pp. 1–16, 2017.
[25] X. Jin, A. Prado, and S. K. Agrawal, "Retraining of human gait - are lightweight cable-driven leg exoskeleton designs effective?," *IEEE Trans. Neural Syst. Rehabil. Eng.*, vol. 26, no. 4, pp. 847–855, Apr. 2018.
[26] Z. Zhou et al., "Concept and prototype design of a soft knee exoskeleton with continuum structure (SoftKEX)," in *Proc. Int. Conf. Intell. Robot. Appl.*, 2019, pp. 173–182.
[27] Z. Zhou, Z. Wang, and Q. Wang, "On the design of rigid-soft hybrid exoskeleton based on remote cable actuator for gait rehabilitation," in *Proc. IEEE/ASME Int. Conf. Adv. Intell. Mechatron.*, 2020, pp. 1902–1907.
[28] X. Liu et al., "Real-time mode recognition based assistive torque control of bionic knee exoskeleton for sit-to-stand and stand-to-sit transitions," *Robot. Auton. Syst.*, vol. 119, pp. 209–220, 2019.
[29] M. W. Whittle, *Gait Analysis: an Introduction*, 3rd ed. Oxford, UK: Butterworth-Heinemann, 2002.

Zilu Wang received the B.S. degree in sports rehabilitation from Tianjin Medical University, Tianjin, China, in 2019. He is currently working toward the Ph.D. degree in biomedical engineering with the College of Engineering, Peking University, Beijing, China.

His research interests include wearable robotics and rehabilitation engineering.

Zhihao Zhou (Member, IEEE) received the B.E. degree in mechanical design, manufacturing and automation from the China University of Geosciences, Beijing, China, in 2012, and the Ph.D. degree in dynamics and control from Peking University, Beijing, China, in 2017.

He then joined the Beijing Innovation Center for Engineering Science and Advanced Technology, Peking University as a Postdoctoral Researcher. He is currently an Assistant Professor with the Institute for Artificial Intelligence, Peking University. His research interests include wearable systems and rehabilitation robots.

Lecheng Ruan received the B.S. degree in robotics from the Harbin Institute of Technology, Harbin, China, in 2015, and the Ph.D. degree in mechanical engineering from the University of California, Los Angeles, CA, USA, in 2020.

He is currently affiliated with the Beijing Institute for General Artificial Intelligence and Peking University, Beijing, China. He is also a Member of the National Key Laboratory of General Artificial Intelligence. His research interests include control and optimization, mechatronics, robotics, perception, and signal processing.

Xiaojie Duan received the B.S. degree in chemistry from Lanzhou University, Lanzhou, China, in 2002, and the Ph.D. degree in chemistry from Peking University, Beijing, China, in 2007.

From 2008 to 2013, she worked with Harvard University, Cambridge, MA, USA, as a Postdoctoral Scholar. She is currently an Associate Professor with the College of Future, Peking University. She focuses on developing materials and technologies for soft and multimodality neural interfacing.

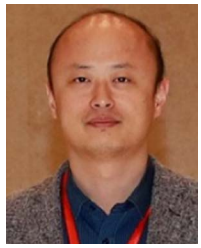

Qining Wang (Senior Member, IEEE) received the Ph.D. degree in dynamics and control from Peking University, Beijing, China, in 2009.

He has authored or coauthored more than 200 scientific papers in international journals and refereed conference proceedings. He is currently a Full Professor and the Vice Dean of the College of Engineering, Peking University. His research interests include wearable robotics and human–machine interfaces.

Dr. Wang was an Associate Editor for IEEE Robotics and Automation Magazine from 2016 to 2018, and a Technical Editor for IEEE/ASME TRANSACTIONS ON MECHATRONICS from 2017 to 2020. He has been an Associate Editor for *Robotica* since 2018 and an Associate Editor for IEEE TRANSACTIONS ON MEDICAL ROBOTICS AND BIONICS since 2018.